Journal of Physics: Condensed Matter

PAPER

Laser-induced enhancement of vertical polarization in ferroelectric bilayer WTe_2

To cite this article: Qing Yang *et al* 2022 *J. Phys.: Condens. Matter* **34** 424003

IOP Publishing Journal of Physics: Condensed Matter
J. Phys.: Condens. Matter **34** (2022) 424003 (7pp) https://doi.org/10.1088/1361-648X/ac885b

Laser-induced enhancement of vertical polarization in ferroelectric bilayer WTe_2

Qing Yang[1], **Chenchen Song**[1,2] **and Sheng Meng**[1,2,3,*]

[1] Beijing National Laboratory for Condensed Matter Physics and Institute of Physics,Chinese Academy of Sciences, Beijing 100190, People's Republic of China
[2] School of Physical Sciences, University of Chinese Academy of Sciences, Beijing 100049, People's Republic of China
[3] Songshan Lake Materials Laboratory, Dongguan 523808, People's Republic of China

E-mail: smeng@iphy.ac.cn

Received 26 April 2022, revised 20 July 2022
Accepted for publication 9 August 2022
Published 18 August 2022

Abstract

Light–matter interaction is one of the key means to manipulate the structural and electronic properties of materials, especially in two-dimensional (2D) layered materials, which are optically accessible due to their atomic thickness. We propose that an ultrashort laser pulse could drastically enhance the ferroelectric polarization of bilayer WTe_2 by our real-time time-dependent density functional theory simulations. It is noted that bilayer WTe_2 is a 2D sliding ferroelectric material recently discovered whose vertical polarization can be controlled by a slight horizontal displacement. We demonstrate that interlayer sliding and compression are simultaneously achieved upon illumination of linearly polarized near-infrared laser pulse, leading to an ultrafast electric polarization enhancement by ∼230% within hundreds of femtosecond. Two major contributions have been identified: (a) the piezoelectric effect due to laser-induced interlayer compression, caused by interlayer charge transfer and dipole-dipole interaction; (b) the interlayer sliding along the opposite direction of ferroelectric switching, induced by inhomogeneous excited carrier distribution and specific electron-phonon couplings. This work provides new insights on controlling ferroelectricity of layered materials, which may extend to other van der Waals bilayers and even bulk materials.

Supplementary material for this article is available online

Keywords: ferroelectric, sliding, compression, laser-induced, bilayer WTe_2

(Some figures may appear in colour only in the online journal)

1. Introduction

Ferroelectric (FE) materials exhibit spontaneous electric polarization due to the lack of inversion symmetry, such that its magnitude and direction can be switched by an external electric field [1, 2]. The bi-stable states of FE materials with equivalent '0' and '1' states, have a wide range of applications such as non-volatile memories, sensors and field-effect transistors [3, 4]. Optical control of structural and electronic properties of materials allows a new gateway to modulate ferroelectricity at the ultrafast time scale [5, 6]. In this regard, two-dimensional (2D) layered materials are more attractive because of the atomic-scale local switching [7]. Recent studies show that terahertz or infrared laser sources, which provide ultrafast pulsed electric fields, are expected to modulate the FE polarization [8]. For example, Miyamoto *et al* reported an 11.3% transient interlayer contraction of bilayer h-BN due to an interlayer dipole-dipole interaction, leading to the transient enhancement of FE polarization [9]. Later on, they also demonstrated that nonlinear couplings between optical phonons in monolayer SnTe, a 2D in-plane FE material, would

* Author to whom any correspondence should be addressed.

produce a polarization oscillation of in-plane polarization in response to out-of-plane phonons [10]. Therefore, laser modulation of ferroelectricity in 2D layered materials (such as FE phase transition or polarization enhancement) is a promising avenue for both materials science and photonics. Since 2013, ferroelectricity has been discovered in a series of 2D materials including In_2Se_3 [11], $CuInP_2S_6$ [12] and group IV–VI monolayers [13]. However, there are few studies on the modulation of ferroelectricity in 2D layered materials by ultrafast laser.

Recently, a new FE switching mechanism known as sliding ferroelectricity, where the modulation of FE polarization was caused by interlayer sliding, was first proposed in bilayer h-BN in 2017 [14] and confirmed experimentally in 2021 [15, 16]. The same sliding ferroelectricity was reported in rhombohedral stacked bilayer transition metal dichalcogenides experimentally [17] and two-dimensional MoA_2N_4 (A = Si or Ge) bilayers theoretically [18]. In addition, room-temperature vertical ferroelectricity was demonstrated in the bilayer and trilayer WTe_2 for the first time, which can be switched by gate electrodes [19]. Later, first-principles calculations gave the evidence that the weak FE in the bilayer and trilayer WTe_2 should be switchable by interlayer sliding [20]. Sie *et al* demonstrated that terahertz light pulses could be used to induce terahertz-frequency interlayer shear strain with a large amplitude in Weyl semimetal WTe_2, leading to a topologically distinct metastable phase [21]. Meanwhile, Guan *et al* reported that the switchable interlayer sliding can be achieved in response to a linear polarized laser in bulk WTe_2 by time-dependent density function theory molecular dynamic (TDDFT-MD) [22]. However, bulk Weyl semimetal WTe_2 has no ferroelectricity due to that the itinerant electrons screen out electrostatic forces between ions [19]. The ferroelectricity of layered WTe_2 was regulated by conventional gated electric fields rather than new ways and there are no studies on laser-induced modulation of ferroelectricity in layered WTe_2. Therefore, a quantitative analysis of the evolution of atomic and electronic dynamics in bilayer WTe_2 upon photoexcitation is highly desirable.

Motivated by the above discussions, this work aims at giving a new insight of modulation of ferroelectricity during laser drive interlayer dynamics of bilayer WTe_2. We find that the FE polarization of bilayer WTe_2 can be significantly enhanced in hundreds of femtoseconds by laser illumination based on *ab initio* TDDFT-MD quantum simulations. The dynamical atomic trajectories reveal that the interlayer sliding and compression take place simultaneously, leading to the enhancement of vertical polarization. Our findings not only provide a new way to control ferroelectricity of sliding FEs, but also give a framework to control the ferroelectricity in 2D FE materials by ultrafast laser excitation in other transition metal dichalcogenides and layered materials.

2. Methods

Our density function theory (DFT) calculations are performed based on Vienna *ab initio* simulation package [23]. The exchange-correlation effect is described within the generalized gradient approximation in the Perdew–Burke–Ernzerhof (PBE) functional [24], together with the projector augmented wave potentials [25]. The kinetic energy cutoff is set to 400 eV, and the total energy convergence criterion 10^{-6} eV is used. The optimized convergence criterion for atomic coordinates is less than 0.001 eV $Å^{-1}$ for forces on each atom. For all calculations, the PBE-D3 method of Grimme with Becke–Jonson damping is applied for the interlayer van der Waals interaction [26], and a vacuum space along the z axis is larger than 14 Å to avoid spurious interactions. The $11 \times 7 \times 1$ Monkhorst–Pack k-meshes are used to sample the Brillouin zone for all structures presented in this study. Dipole moment corrections are employed to calculate the vertical polarization. The FE transition path and energy barrier are calculated by using the nudged elastic band (NEB) method.

The TDDFT-MD calculations are performed in a time-dependent *ab initio* package [27, 28]. Numerical atomic orbitals with double zeta polarization are employed as the basis set. The electron-nuclear interactions are described by PBE functional. The plane-wave energy cutoff of 250 Ry is adopted. The $6 \times 5 \times 1$ k-point grid is used to sample the Brillouin zone and the PBE-D3 method of Grimme with Becke–Jonson damping is applied. The coupling between atomic and electronic motions is governed by the Ehrenfest approximation. During molecular dynamic simulations, the evolution time step is 50 attoseconds for both electrons and ions in a micro-canonical ensemble (NVE).

3. Results

3.1. Ferroelectricity in bilayer WTe_2

The bi-stable FE geometric structures of bilayer WTe_2 defined as State FE1 and State FE2 are shown in figure 1(a), with the lattice parameters $a = 3.52$ Å and $b = 6.30$ Å from our first-principles calculations, which are consistent with the experimental values (where $a = 3.48$ Å and $b = 6.27$ Å) [29]. The State FE2 with the reversed vertical polarization along the z axis can be obtained by a mirror operation of State FE1 in the center of xy plane. However, it is impossible to switch the FE polarization through mirror symmetry operation in practice. On the other hand, we find that a slight interlayer sliding along the horizontal y axis may be a feasible pathway for FE switch, transforming State FE1 (polarization aligned in the z axis) to State FE2 (polarization aligned in the $-z$ axis), as depicted in figure 1(a). As illustrated for State FE1, such a slight sliding is feasible along y axis as the horizontal distance between Te1 and Te3, $-\Delta 1 = y(\mathrm{Te1}) - y(\mathrm{Te3}) = -0.20$ Å, is different from the horizontal distance between Te2 and Te4, $-\Delta 2 = y(\mathrm{Te2}) - y(\mathrm{Te4}) = -0.15$ Å. State FE2 can be obtained by sliding the upper layer along the y axis by a distance of $\Delta 1 + \Delta 2 = 0.35$ Å, where the horizontal distance of $y(\mathrm{Te1}) - y(\mathrm{Te3})$ and $y(\mathrm{Te2}) - y(\mathrm{Te4})$ in State FE2 have been changed to $\Delta 2$ and $\Delta 1$, respectively. The inequality of $\Delta 1$ and $\Delta 2$ shows the inversion symmetry breaking along the z axis, leading to the vertical ferroelectricity of bilayer WTe_2.

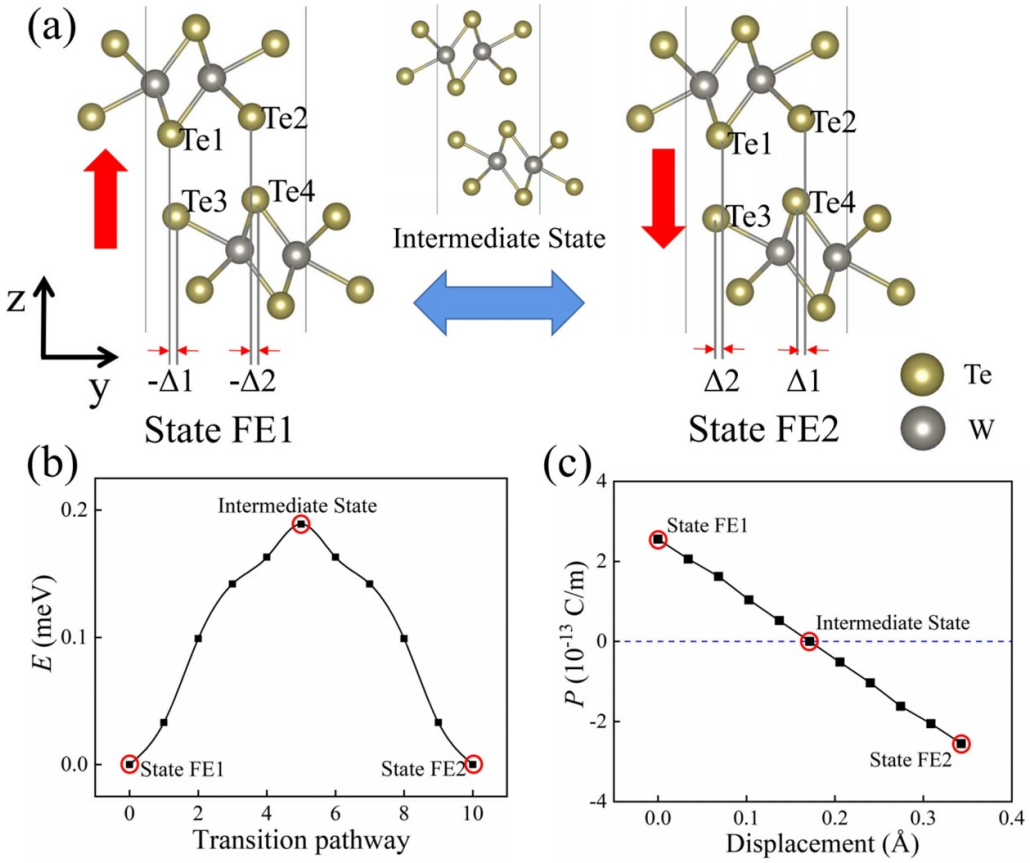

Figure 1. (a) Ferroelectric switching pathway of bilayer WTe_2 form State FE1 to State FE2. Gray (dark yellow) spheres denote W (Te) atoms. The red arrows represent the vertical polarization direction. (b) The ferroelectric switching pathway and the energy barrier for bilayer WTe_2. (c) Dependence of the out-of-plane polarization (P) on the displacement along the y axis.

In addition, the vertical polarization of bilayer WTe_2 is calculated by DFT with dipole corrections. Our results show that the vertical FE polarization of such a bilayer WTe_2 is about 2.44×10^{11} e cm^{-2} (FE polarization in 2D is 2.55×10^{-13} C m^{-1}), which is in excellent agreement with the previous experimental (2×10^{11} e cm^{-2}) and calculated values (3.2×10^{11} e cm^{-2}) [20]. The band structure with spin-orbital coupling of bilayer WTe_2 is shown in figure S1, where the Rashba splitting at the conduction band minimum along $\Gamma \rightarrow X$ direction, is another evidence of inversion symmetry breaking, leading to the presence of vertical polarization. The FE switching pathway and minimum energy barrier are calculated based on NEB method, as shown in figure 1(b). We find that the FE switching energy barrier is only about 0.2 meV per unit cell induced by interlayer sliding. The intermediate state shown in figure 1(a), where the horizontal distances are defined as y(Te1) − y(Te3) = (Δ1 − Δ2)/2 = −0.025 Å and y(Te2) − y(Te4) = (Δ2 − Δ1)/2 = 0.025 Å, has the inversion symmetry with no net polarization. The dependence of FE polarization on the displacement of upper layer is illustrated in figure 1(c). The results show that the polarization varies linearly with the horizontal displacement of upper layer, where the start point is the State FE1 and the end point (displacement (Δ1 + Δ2) = 0.35 Å) is the State FE2, and the intermediate state (displacement of (Δ1 + Δ2)/2 = 0.175 Å) has no FE polarization. The charge density differences (CDDs) of State FE1 and State FE2 between the upper and lower layers are depicted in figures S2(a) and (b), where the yellow (blue) area indicates charge accumulation (depletion). There is charge transfer between the two sheets due to the nonequivalence of charge accumulation and depletion regions. Interestingly, an inversion between the CDDs of the two FE states (black cycles illustrated in figure S2), is fully consistent with the FE polarization directions shown in figure 1(a).

3.2. *Laser induced the enhancement of polarization*

To study the photoelectronic responses of bilayer WTe_2, the Gaussian-type laser pulse with a time-dependent electric field $E(t) = E_0 \cos(\omega t) \exp\left[\frac{-(t-t_0)^2}{2\sigma^2}\right]$ and a wavelength of 2106 nm (photon energy ∼0.6 eV), is adopted in our calculations. The laser pulse is linearly polarized along the y axis, perpendicular to the out-of-plane FE polarization. As illustrated in figure S2, the peak intensity and full width at half maximum of applied laser field are set as 0.152×10^{10} W cm^{-2} and 10 fs, respectively. There are 0.3% of valence electrons excited to the conduction bands after laser pulse ends (at t = 80 fs) as shown in figure S2.

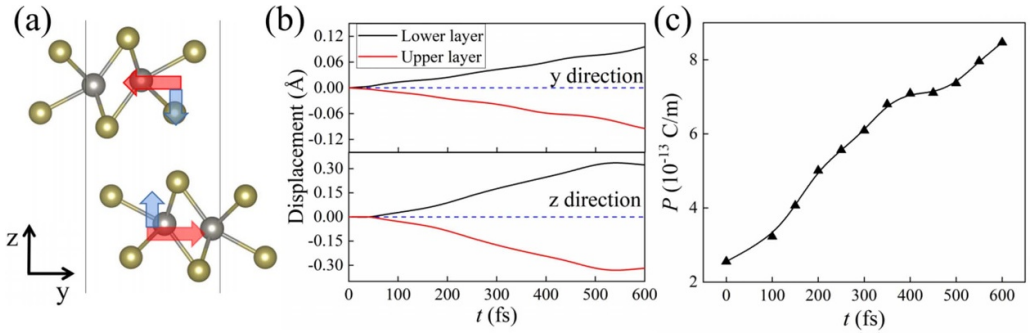

Figure 2. (a) Laser-induced interlayer displacement. Red and blue arrows represent the displacement along the y and z axis, respectively. (b) Time (t) dependent interlayer shear displacement along the y and z axis respectively for the upper and lower layer. (c) Time (t) dependent FE polarization (P) of bilayer WTe_2.

Here, we show that the interlayer sliding and compression occur simultaneously upon the photoexcitation of laser pulse. To describe the interlayer displacement, we defined the average motions as:$\Delta y(a,t) = \frac{1}{N}\sum_{i=1}^{N}[y_i(a,t) - y_i(a,0)]$, $a = x,y,z$, where $y_i(a,t)$ is the time-dependent position of atom i along the a axis ($a = x,y,z$), and $y_0(a,t)$ is the ground state position of atom i along the a axis ($a = x,y,z$). The atoms of lower and upper layer are calculated separately to estimate the interlayer shear displacements.

Figures 2(a) and (b) show the shear displacements and directions of upper and lower layer when the near-infrared laser pulse is applied. It is clear that the upper and lower layer moves in opposite directions with the nearly identical speed (the upper layer moving along the $-y$ and $-z$ axis and the lower layer moving along the y and z axis), leading to the simultaneous interlayer sliding and contraction. On the one hand, the average speed of interlayer horizontal sliding is $\sim$14 m s^{-1}, which is defined as the displacement along the y axis. The relative displacement reaches 0.095 Å at $t = 600$ fs as depicted in figure 2(b). After 600 fs, the interlayer sliding would continue with time, which has been reported in previous experiments [21]. On the other hand, we also find that the interlayer compression starts at the end of laser pulse and reaches a maximum of about 0.67 Å at 540 fs with an average speed of $\sim$22 m s^{-1}. Subsequently, the interlayer charge transfer and repulsion force increases sharply due to the sharp reduction of the interlayer distance. Therefore, the displacement along the z axis is reversed after 540 fs, leading to the interlayer distance increasing.

To study the influence of interlayer displacement on ferroelectricity of bilayer WTe_2, we calculated the time-dependent FE polarization as shown in figure 2(c). The maximum vertical polarization value is $\sim 8.4 \times 10^{-13}$ C m^{-1} at $t = 600$ fs, which is $\sim$230% larger than the polarization value in the ground state at $t = 0$ fs. It is noted that the vertical FE polarization caused by interlayer sliding is small due to the depolarization field, e.g. in bilayer WTe_2 and h-BN, which limits its application in microelectronic devices. Here, we demonstrate that the laser pulse can effectively control the enhancement of FE polarization in bilayer WTe_2, which is expected to be a new gateway for regulating the FE polarization in 2D layered materials.

3.3. Laser induced interlayer compression

To explore the influence of interlayer compression induced by the laser pulse on FE polarization, we analyze the displacement along the z axis while ignoring the interlayer sliding in the horizontal direction. We then monitor the interlayer distance, which is defined by the perpendicular distance between the W atoms of different layers through the TDDFT-MD simulation. The original interlayer distance d is 6.74 Å as depicted in figure 3(a). By comparing the time evolution of the interlayer distance with and without laser pulse, a considerable compression of more than 0.67 Å (10% of the original interlayer distance) in 540 fs was shown in figure 3(b). After $t = 540$ fs, the interlayer distance increases again because of the dissociation of the two WTe_2 sheets. The inhomogeneous carrier distribution along the z axis due to the spontaneous vertical polarization will introduce a built-in electric field in bilayer WTe_2. Simultaneously, the enhanced interlayer charge transfer and dipole-dipole interaction would induce asymmetric charge distribution, leading to the interlayer compression.

It is worth noting that the vertical FE polarization can be enhanced due to the increased interlayer charge transfer if the interlayer distance is compressed, as depicted in figures 3(c) and (d). The wavy patterns in figures 3(c) and (d) indicate that the system is stabilized with oscillating interlayer distances after the rapid light-induced compression process. Bilayer WTe_2 is FE with vertical polarization because of the interlayer charge transfer, i.e. the centers of the positive and negative do not overlap. The vertical polarization will be changed and regulated when the stress is applied along the z direction. Since piezoelectricity is the electric charge that accumulates in certain solid materials in response to applied mechanical stress, bilayer WTe_2 thus has piezoelectricity along the z axis. The enhancement of FE polarization induced by interlayer compression, which can increase by about 64.3% at $d \sim 6.54$ Å, with a contraction of more than 0.2 Å (3% of the original interlayer distance). After $t = 200$ fs, the saturation of polarization value may be caused by the saturation of charge transfer between the two sheets.

Interlayer compression not only increases the FE polarization of bilayer WTe_2, but also changes the potential energy

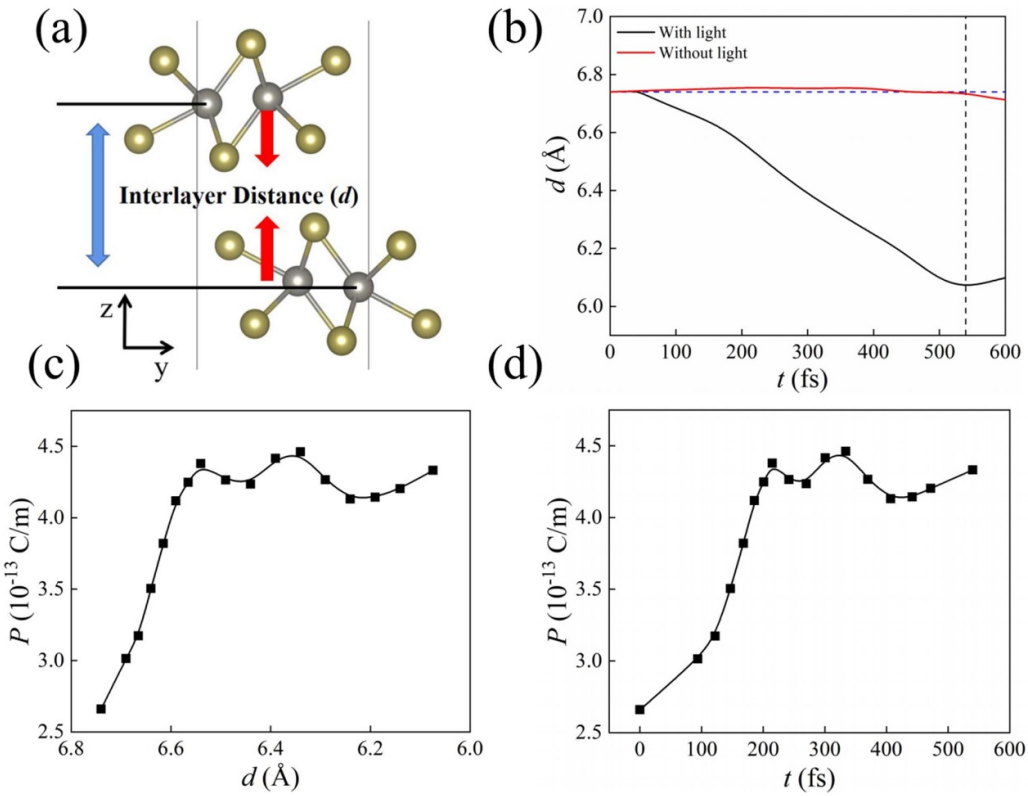

Figure 3. (a) Laser-induced interlayer compression. (b) Interlayer distance (d) as a function of time (t). The dotted (blue) line and the dotted (black) line show the initial interlayer distance and minimum interlayer distance at $t = 540$ fs, respectively. (c) FE polarization (P) as a function of displacement along z axis. (d) FE polarization (P) as a function of time (t).

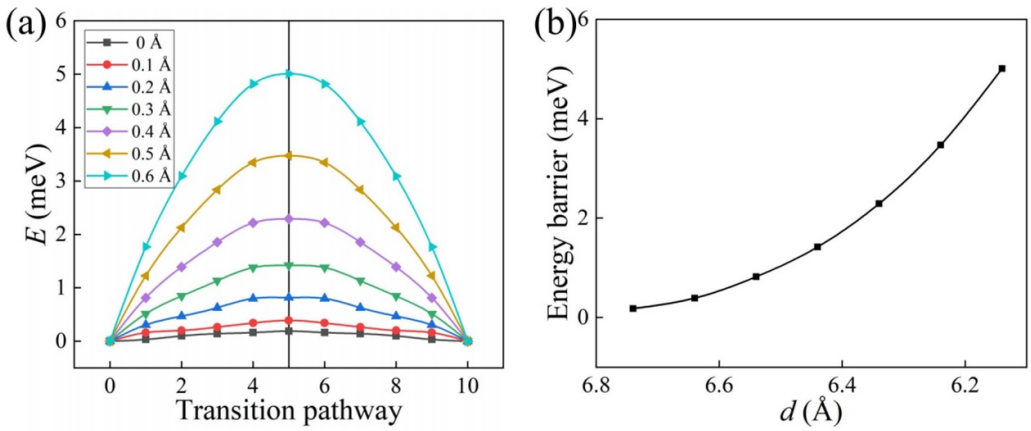

Figure 4. (a) Potential energy surfaces of FE phase transition in different interlayer displacements along the z axis. (b) Energy barriers dependent on the interlayer distance (d).

surface of its FE phase transition. Figure 4(a) shows the potential energy surfaces of FE phase transition change with interlayer distance, which are calculated by NEB method. The energy barrier rapidly increases with the decrease of interlayer distance due to the enhanced interlayer coupling, and reaches 5 meV, an order of magnitude larger than the original energy barrier at the contraction of 0.6 Å, as illustrated in figure 4(b). The enhancement of FE polarization and energy barriers induced by laser pulses implies that we obtain a more stable FE phase to resist environmental disturbances.

3.4. Laser induced interlayer sliding

The polarization would not be increased by ∼230% due to the interlayer compression alone. It means that the interlayer sliding also plays an important role in the enhancement of FE polarization. Figure 5(a) shows the time-dependent horizontal displacement of lower layer, which varies almost linearly with time, while the upper layer is considered to be fixed. The results show that the lower layer is sliding along the y axis, which is opposite to the FE phase transition direction.

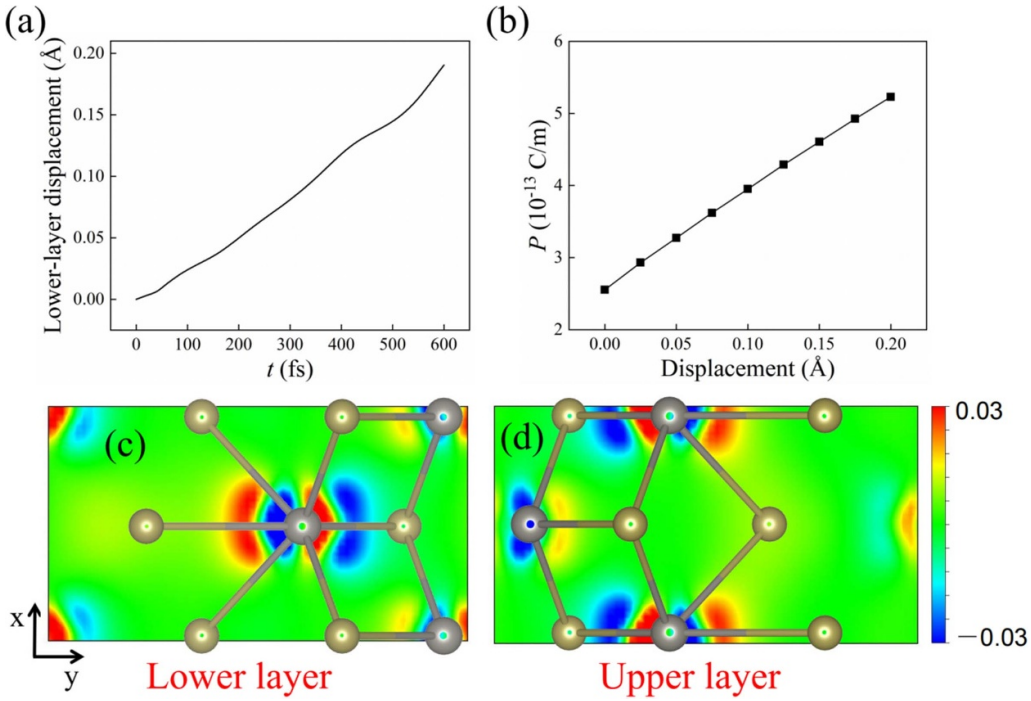

Figure 5. (a) The lower layer displacement relative to the upper layer. (b) Vertical polarization (P) as a function of lower layer displacement. Charge density differences (CDDs) at the plane of W atoms of lower (c) and upper layer (d) between the ground state and excitation state at $t = 100$ fs. The red (blue) region represents the accumulation (depletion) in charge density.

The reverse displacement, where the horizontal displacement is about 0.19 Å at $t = 600$ fs, causes an enhancement of FE polarization as shown in figure 5(b). It is clear that the FE polarization, which is nearly linear with the horizontal displacement, can increase by ∼100% upon the displacement of 0.19 Å. Our results demonstrate that the increase of vertical FE polarization in bilayer WTe_2 is due to the combination of interlayer compression and sliding. As shown in figure S3, when the lower layer is sliding continuously under the laser pulse polarized along the y axis, the interlayer voltage will oscillate and generate an alternating current output signal, which can be used as a nanogenerator, where the variations in the potential of the bilayer can be used to drive the flow of electrons and to harvest energy.

In order to confirm further that the interlayer sliding is induced by the photoexcited electrons, the laser-induced net charges and charge transfer distributed in real-space can be described by CDD as depicted in figures 5(c) and (d). Here, time-dependent CDD is defined as $\Delta\rho(\boldsymbol{r},t) = \rho(\boldsymbol{r},t) - \rho(\boldsymbol{r},0)$, where $\rho(\boldsymbol{r},t)$ is the charge density at time $t = 100$ fs is shown on the plane cutting along the upper and lower layer of the unit cell, respectively. The inhomogeneous carrier distribution of upper and lower layer introduces a built-in electric field along the $-y$ axis, which induces the displacement along the $-y$ axis as shown in figure 5(c). On the contrary, figure 5(d) shows that the asymmetry carrier distribution introduces the opposite electric field and induce the opposite displacement, simultaneously. Therefore, the opposite displacement of two sheets enhance the vertical FE polarization effectively. As we know, the laser modulation of materials is dependent on laser intensity, so we also test the modulation of atomic structures in bilayer WTe_2 with different laser intensities. As shown in figures S5(a) and (b), with the increase of laser intensity, the atomic movements are accelerated and are linearly dependent on the laser intensity. A similar phenomenon also occurs in perpendicular movements as shown in figures S5(c) and (d). This confirms that the displacements of bilayer WTe_2 can be controlled by selecting a proper intensity of laser pulses.

4. Conclusion

In summary, our *ab initio* TDDFT-MD simulations reveal that the vertical FE polarization of bilayer WTe_2 can increase up to ∼230% upon laser excitation, which is caused by the synergistic action of interlayer compression and sliding. The piezoelectric effect and laser-induced interlayer compression, caused by interlayer charge transfer and dipole-dipole interaction along the z axis, contributes an enhancement of FE polarization by about 64.3%. Meanwhile, the energy barrier rapidly increases to ∼5 meV (an order of magnitude larger than that in the ground state) with the decrease of interlayer separation, leading to a more stable FE phase to resist environmental disturbances. Importantly, the interlayer sliding along the opposite direction of FE switching, induced by inhomogeneous carrier distribution and specific electron-phonon couplings, results in the enhancement of FE polarization by another ∼100%. Our work provides a new perspective on modulating the FE polarization of layered materials, and similar phenomena induced by laser pulses is predicted to exist widely in various bilayers (BN, MoS_2, etc) or even in bulk phases.

Data availability statement

The data that support the findings of this study are available upon reasonable request from the authors.

Acknowledgments

We acknowledge partial financial support from the National Key Research and Development Program of China (No. 2021YFA1400201), National Natural Science Foundation of China (No. 12147130), China Postdoctoral Science Foundation (No. 2021M693371).

Conflict of interest

There are no conflicts to declare.

ORCID iDs

Qing Yang https://orcid.org/0000-0003-2358-411X
Sheng Meng https://orcid.org/0000-0002-1553-1432

References

[1] Anderson P W and Blount E I 1965 Symmetry considerations on martensitic transformations: "ferroelectric" metals? *Phys. Rev. Lett.* **14** 217
[2] Bune A V, Fridkin V M, Ducharme S, Blinov L M, Palto S P, Sorokin A V, Yudin S G and Zlatkin A 1998 Two-dimensional ferroelectric films *Nature* **391** 874
[3] Scott J F 2007 Applications of modern ferroelectrics *Science* **315** 954
[4] Wen Z, Li C, Wu D, Li A and Ming N 2013 Ferroelectric-field-effect-enhanced electroresistance in metal/ferroelectric/semiconductor tunnel junctions *Nat. Mater.* **12** 617
[5] Lian C, Ali Z A, Kwon H and Wong B M 2019 Indirect but efficient: laser-excited electrons can drive ultrafast polarization switching in ferroelectric materials *J. Phys. Chem. Lett.* **10** 3402
[6] Henstridge M, Först M, Rowe E, Fechner M and Cavalleri A 2022 Nonlocal nonlinear phononics *Nat. Phys.* **18** 457
[7] Fu H and Cohen R E 2000 Polarization rotation mechanism for ultrahigh electromechanical response in single-crystal piezoelectrics *Nature* **403** 281
[8] Cavalleri A, Wall S, Simpson C, Statz E, Ward D W, Nelson K A, Rini M and Schoenlein R W 2006 Tracking the motion of charges in a terahertz light field by femtosecond x-ray diffraction *Nature* **442** 664
[9] Miyamoto Y, Zhang H, Miyazaki T and Rubio A 2015 Modifying the interlayer interaction in layered materials with an intense IR laser *Phys. Rev. Lett.* **114** 116102
[10] Shin D, Sato S A, Hübener H, De Giovannini U, Park N and Rubio A 2020 Dynamical amplification of electric polarization through nonlinear phononics in 2D SnTe *npj Comput. Mater.* **6** 182
[11] Ding W, Zhu J, Wang Z, Gao Y, Xiao D, Gu Y, Zhang Z and Zhu W 2017 Prediction of intrinsic two-dimensional ferroelectrics in In_2Se_3 and other III_2-VI_3 van der Waals materials *Nat. Commun.* **8** 14956
[12] Belianinov A, He Q, Dziaugys A, Maksymovych P, Eliseev E, Borisevich A, Morozovska A, Banys J, Vysochanskii Y and Kalinin S V 2015 $CuInP_2S_6$ room temperature layered ferroelectric *Nano Lett.* **15** 3808
[13] Wu M and Zeng X C 2016 Intrinsic ferroelasticity and/or multiferroicity in two-dimensional phosphorene and phosphorene analogues *Nano Lett.* **16** 3236
[14] Li L and Wu M 2017 Binary compound bilayer and multilayer with vertical polarizations: two-dimensional ferroelectrics, multiferroics, and nanogenerators *ACS Nano* **11** 6382
[15] Stern M V, Waschitz Y, Cao W, Nevo I, Watanabe K, Taniguchi T, Sela E, Urbakh M, Hod O and Shalom M B 2021 Interfacial ferroelectricity by van der Waals sliding *Science* **372** 1462
[16] Yasuda K, Wang X, Watanabe K, Taniguchi T and Jarillo-Herrero P 2021 Stacking-engineered ferroelectricity in bilayer boron nitride *Science* **372** 1458
[17] Wang X, Yasuda K, Zhang Y, Liu S, Watanabe K, Taniguchi T, Hone J, Fu L and Jarillo-Herrero P 2022 Interfacial ferroelectricity in rhombohedral-stacked bilayer transition metal dichalcogenides *Nat. Nanotechnol.* **17** 367
[18] Zhong T, Ren Y, Zhang Z, Gao J and Wu M 2021 Sliding ferroelectricity in two-dimensional MoA_2N_4 (A = Si or Ge) bilayers: high polarizations and moiré potentials *J. Mater. Chem.* A **9** 19659–63
[19] Fei Z, Zhao W, Palomaki T A, Sun B, Miller M K, Zhao Z, Yan J, Xu X and Cobden D H 2018 Ferroelectric switching of a two-dimensional metal *Nature* **560** 336
[20] Yang Q, Wu M and Li J 2018 Origin of two-dimensional vertical ferroelectricity in WTe_2 bilayer and multilayer *J. Phys. Chem. Lett.* **9** 7160
[21] Sie E J *et al* 2019 An ultrafast symmetry switch in a Weyl semimetal *Nature* **565** 61–66
[22] Guan M-X, Wang E, You P-W, Sun J-T and Meng S 2021 Manipulating weyl quasiparticles by orbital-selective photoexcitation in WTe_2 *Nat. Commun.* **12** 1885
[23] Kresse G and Furthmüller J 1996 Efficient iterative schemes for *ab initio* total-energy calculations using a plane-wave basis set *Phys. Rev.* B **54** 11169–86
[24] Perdew J P, Burke K and Ernzerhof M 1996 Generalized gradient approximation made simple *Phys. Rev. Lett.* **77** 3865
[25] Blöchl P E 1994 Projector augmented-wave method *Phys. Rev.* B **50** 17953–79
[26] Grimme S, Antony J, Ehrlich S and Krieg H 2010 A consistent and accurate *ab initio* parametrization of density functional dispersion correction (DFT-D) for the 94 elements H-Pu *J. Chem. Phys.* **132** 154104
[27] Meng S and Kaxiras E 2008 Real-time, local basis-set implementation of time-dependent density functional theory for excited state dynamics simulations *J. Chem. Phys.* **129** 054110
[28] Lian C, Guan M, Hu S, Zhang J and Meng S 2018 Photoexcitation in solids: first-principles quantum simulations by real-time TDDFT *Adv. Theory Simul.* **1** 1800055
[29] Ali M N *et al* 2014 Large, non-saturating magnetoresistance in WTe_2 *Nature* **514** 205